

---

# Study of Deep Generative Models for Inorganic Chemical Compositions

---

**Yoshihide Sawada**  
Panasonic Corporation  
sawada.yoshihide@jp.panasonic.com

**Koji Morikawa**  
Panasonic Corporation  
morikawa.koji@jp.panasonic.com

**Mikiya Fujii**  
Panasonic Corporation  
fujii.mikiya001@jp.panasonic.com

## Abstract

Generative models based on generative adversarial networks (GANs) and variational autoencoders (VAEs) have been widely studied in the fields of image generation, speech generation, and drug discovery, but, only a few studies have focused on the generation of inorganic materials. Such studies use the crystal structures of materials, but material researchers rarely store this information. Thus, we generate chemical compositions without using crystal information. We use a conditional VAE (CondVAE) and a conditional GAN (CondGAN) and show that CondGAN using the bag-of-atom representation with physical descriptors generates better compositions than other generative models. Also, we evaluate the effectiveness of the Metropolis-Hastings-based (MH) atomic valency modification and the extrapolation performance, which is important to material discovery.

## 1 Introduction

In recent years, generative models based on generative adversarial networks (GANs) [11] and variational autoencoders (VAEs) [17] have been widely studied in the fields of image generation [6], speech generation [28], and drug discovery [33]. Drug discovery has been rich with studies resulting from the collaboration of machine learning and materials science to generate valid organic molecules by the use of SMILES or graph representations [30, 33, 21]. However, there have been only a few studies focusing on inorganic materials [25, 14, 24].

Nouira et al. [25] introduces geometric constraints and shows that their method can produce stable structures for particular chemicals. Also, Hoffmann et al. [14] and Noh et al. [24] propose a VAE-based method to generate 3D crystal structures. Since crystal information is known to improve the performance of predictions [34, 35, 32, 7], these methods are likely to generate valid inorganic molecules.

Physical properties are, in principle, governed by crystal structures and electron distributions, which can be explored by X-ray diffraction techniques and first-principles calculations. These methodologies, however, are not so feasible and are time-consuming, therefore only chemical compositions and observed physical properties are stored for the rapid exploration of new materials. These problems have led us to attempt the generation of chemical compositions without using crystal information.

Our goal is to achieve an innovative design, a so-called Inverse Material Design (IMD) [16, 30], of inorganic materials. This design predicts promising chemical compositions when the desired properties are given, whereas the conventional development of materials is based on physical laws and physical properties predicted from chemical compositions, crystal structures, and electron

distributions. To achieve this design, there are two approaches to generative models, which are reinforcement learning (RL) + unsupervised models [12, 31, 8] and conditional models [9, 20, 3]. RL + unsupervised models use simulators for obtaining rewards (e.g., drug-likeness) and the unsupervised generative models generate samples to maximize the rewards. Such models have been widely used for the generation of organic molecules. However, the inorganic molecules generated by these models have to be evaluated by computationally expensive density functional theory (DFT) calculations that require crystal information. Our study focuses on conditional generative models, such as a conditional GAN (CondGAN) [23, 26] and a conditional VAE (CondVAE) [18, 19].

In material science, it is known that the valence of a chemical composition should become zero. However, standard CondGAN and CondVAE do not preserve this constraint. Madhawa et al. [21] uses a greedy beam search to explore valid graph molecules. We apply a Metropolis Hastings (MH)-based method [4] to balance the atomic valencies of generated compositions.

To construct generative models, we use two different data representations: bag-of-atoms [5] and bag-of-atoms with physical descriptors. Bag-of-atoms is a vector representing the number of each atom included in the composition. By using this representation, we can easily convert to the corresponding composition. The physical descriptors are characteristics computed from the compositions [1], i.e., crystal information is not included in the descriptors.

We experiment with the Materials Project database, which has more than 60,000 inorganic compositions [15], and show that CondGAN and the bag-of-atoms [5] with physical descriptors [1] generate the best compositions. Despite the non-usage of crystal structures, CondGAN( $\mathbf{x}^{bp}$ ) generates compositions around the desired property. Also, we evaluate the effectiveness of the MH-based modification and the extrapolation performance, which is an important skill for IMD [22].

This remainder of this paper is organized as follows. Section 2 describes the bag-of-atoms and physical descriptors. Section 3 describes the generative models, i.e., CondVAE and CondGAN. Section 4 describes the MH-based valency modification. Section 5 and 6 describe the setup and results, respectively, of our experiment. Section 7 discusses our conclusions and direction for future works.

## 2 Representations of Chemical Compositions

As discussed in Sec. 1, we use two different types of data representations: bag-of-atoms [5] and bag-of-atoms with physical descriptors [1]. Let  $\mathbf{x}^b \in \mathbb{R}^{M^b}$  and  $\mathbf{x}^p \in \mathbb{R}^{M^p}$  denote vectors representing the bag-of-atoms and the physical descriptors, respectively, where  $M^b$  and  $M^p$  are the numbers of atoms used in the dataset and physical descriptors, respectively.

$x_i^b$  represents the count of the  $i$ -th atom of the composition. For example, if there are 3 atoms (H, Li, O) used in the dataset and the target composition is H<sub>2</sub>O, then  $\mathbf{x}^b = [2, 0, 1]^\top$ . We can easily convert this representation to the composition.

Table A shows a list of the physical descriptors. In [1], the descriptors of 94 atoms are saved. Using these descriptors, we compute the weighted mean vector,  $\mathbf{x}^p$  (for the example above,  $\mathbf{x}^p = 2/3\mathbf{x}_H + 1/3\mathbf{x}_O$ , where  $\mathbf{x}_H$  and  $\mathbf{x}_O$  are the physical descriptors’ vectors of H and O, respectively). We experimented beforehand and found that this representation provided better performance than others (e.g., weighted variance vector [1]). Note that  $\mathbf{x}^p$  is difficult to convert to the composition, thus we use  $\mathbf{x}^b$  and  $\mathbf{x}^{bp} = [\mathbf{x}^{b^\top}, \mathbf{x}^{p^\top}]^\top$  in our experiments.

## 3 Generative Models

In this section, we describe CondVAE and CondGAN. For simplicity, we represent the input vector by  $\mathbf{x}$ .

### 3.1 Conditional Variational Autoencoder (CondVAE)

In this article, CondVAE has two networks, which are the encoder ( $q_\phi(\cdot)$ ) and decoder ( $p_\theta(\cdot)$ ) [19]. CondVAE trains these networks by minimizing the following equation corresponding to the Evidence

Lower BOund (ELBO) of  $\log p_\theta(\mathbf{x} | y)$ :

$$L_{\text{CondVAE}} = \mathbb{E}_{q_\phi}[\log p_\theta(\mathbf{x} | y, \mathbf{z})] - D_{KL}(q_\phi(\mathbf{z} | \mathbf{x}, y) \| p_\theta(\mathbf{z} | y)), \quad (1)$$

where  $\mathbf{z}$  is the latent vector,  $y$  is the target property,  $\mathbb{E}$  is the expectation, and  $D_{KL}(\cdot \| \cdot)$  is the KL divergence. In this article, we set  $p_\theta(\mathbf{z} | y) = p(\mathbf{z}) = \mathcal{N}(0, \mathbf{I})$  [19].

### 3.2 Conditional Generative Adversarial Network (CondGAN)

We use the auxiliary classifier GAN (ACGAN [26]) as CondGAN. The main difference between the traditional CondGAN and ACGAN is the function of the discriminator, which evaluates if the input is real or fake in the former. In addition to this evaluation, the discriminator in ACGAN classifies the category of the input. The loss function is as follows:

$$L_{\text{CondGAN}} = \mathbb{E}_{\tilde{\mathbf{x}}} [D(\tilde{\mathbf{x}})] - \mathbb{E}_{\mathbf{x}} [D(\mathbf{x})] + \lambda_1 \mathbb{E}_{\tilde{\mathbf{x}}} [(\|\nabla_{\tilde{\mathbf{x}}} D(\tilde{\mathbf{x}})\|_2 - 1)^2] \\ + \lambda_2 \mathbb{E}_{\tilde{\mathbf{x}}} [(y - P(\tilde{\mathbf{x}}))^2] + \lambda_3 \mathbb{E}_{\mathbf{x}} [(y - P(\mathbf{x}))^2], \quad (2)$$

where  $D(\cdot)$  is the output of the real/fake evaluation,  $P(\cdot)$  is the predicted output, and  $\tilde{\mathbf{x}}$  is the output of the generator ( $\tilde{\mathbf{x}} = G(\mathbf{z})$ ),  $\hat{\mathbf{x}} = \epsilon \mathbf{x} + (1 - \epsilon)\tilde{\mathbf{x}}$  ( $\epsilon \sim U[-1, 1]$ , where  $U[-1, 1]$  is the uniform distribution ranging from  $-1$  to  $1$ ).  $\lambda_1$ ,  $\lambda_2$ , and  $\lambda_3$  are hyperparameters. From the first to the third terms are the Wasserstein losses [13], which are known to achieve stable training, whereas the other terms are the auxiliary losses [26]. It should be noted that we use the least square error instead of the cross-entropy loss because the property is not categorical.

## 4 Valency-based Vector Modification

In material science, it is known that the valence of a composition has to become zero. However, the generative models described in the previous section may violate this condition because there is no constraint. We solve this problem by applying an Metropolis-Hastings (MH) method, which is one of the Markov Chain Monte Carlo [4]. MH-based method modifies  $\mathbf{x}^b$  according to the following acceptance probability  $\alpha$ :

$$\alpha(\mathbf{x}_{\text{new}}^b | \mathbf{x}^b) = \min \left( 1, \frac{q(\mathbf{x}^b | \mathbf{x}_{\text{new}}^b) \pi(\mathbf{x}_{\text{new}}^b)}{q(\mathbf{x}_{\text{new}}^b | \mathbf{x}^b) \pi(\mathbf{x}^b)} \right). \quad (3)$$

We use the proposal distribution  $q(\cdot | \cdot)$  as a Gaussian and  $\pi(\cdot)$  as follows:

$$\pi(\mathbf{x}^b) = \max_v (\exp(-(\mathbf{v}^\top \mathbf{x}^b)^\top (\mathbf{v}^\top \mathbf{x}^b))), \quad (4)$$

where  $\mathbf{v}$  is the valence vector that  $v_i$  corresponds to the valence of the  $i$ -th atom. Since there are atoms with multiple valences, we use the maximum value as  $\pi(\cdot)$ .

It is known that the MH method is inefficient when  $\mathbf{x}^b$  is a high dimension [4]. Thus, we compress  $\mathbf{x}^b$  so that it satisfied only the variable  $x_i^b > TH$ . Also, to accelerate the MH search, we sample  $N$  vectors simultaneously and use  $\max(\alpha_j)$ , ( $j = 1, 2, \dots, N$ ) as the acceptance probability. If  $\pi(\cdot) = 1$ , we stop and convert  $\mathbf{x}_{\text{new}}^b$  to the composition.

## 5 Experimental Setup

Before presenting the experimental results, we explain the dataset, network architecture, and hyperparameters. For this implementation, we use Python libraries such as Pymatgen [27], Xenonpy [1], and TensorFlow [2] <sup>1</sup>.

### 5.1 Dataset

For the experiment, we use 69,640 compositions with their formation energies [eV/atom] in the Materials Project [15]. Figure A shows a histogram of the formation energies, which range from  $-4.5$  [eV/atom] to  $4.4$  [eV/atom] (almost  $< 0$  [eV/atom]) and have a bimodal distribution. After removing duplicate compositions, we randomly select 44,040 training data and 5,506 test data. In the evaluation, we generate 256 compositions for each test property.

<sup>1</sup>Sample source code for training CondGAN( $\mathbf{x}^{bp}$ ) is here: <https://github.com/yoshihidesawada/CompGAN>

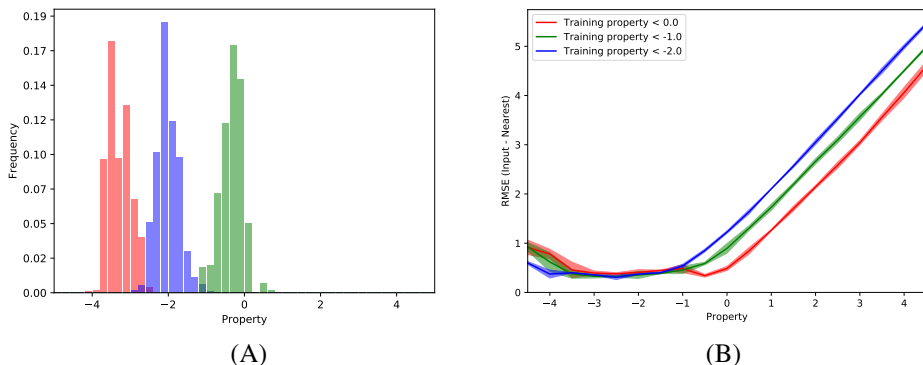


Figure 1: (A) Histogram of the nearest property of the generated compositions. From left to right, the desired properties (input) are  $-3.24$  (red),  $-2.03$  (blue), and  $-0.10$  (green). These property values are not included in the training dataset. (B) Evaluation of the extrapolation. To evaluate the relationship between the extrapolation and the range of training data, we use three types of training data,  $-4.5 \leq y \leq 0.0$  (red),  $-4.5 \leq y \leq -1.0$  (green), and  $-4.5 \leq y \leq -2.0$  (blue).

## 5.2 Network Architecture and Hyperparameters

The number of hidden layers in the generator and the decoder is two while the dimensions of the first and second layers are 60 and 30, respectively. The discriminator and the encoder have the same number of layers and their dimensions are the inverse of the generator/decoder. All models use the fully connected ReLU layer and the optimization is Adam.  $\mathbf{x}^b$  and  $\mathbf{x}^{bp}$  are normalized by  $x_i = (x_i - \min(x_i)) / (\max(x_i) - \min(x_i))$ , where  $\max(x_i)$  and  $\min(x_i)$  are the maximum and minimum, respectively, of the  $i$ -th variable. Also,  $M^b = 89$ ,  $M^p = 58$ ,  $\mathbf{z} \in \mathbb{R}^{10}$ ,  $\lambda_1 = 10$ , and  $\lambda_2 = \lambda_3 = 1$ . The batch and epoch sizes are 256 and 50,000, respectively. To convert the compositions, we use only atoms satisfying  $\mathbf{x}^b > TH$  ( $= 0.03$ ),  $N = 100$ , and normalize their variables to 1. Note that these parameters are empirically determined.

## 6 Experimental Results

### 6.1 Generated Compositions

Table 1 shows the generated compositions of each model. Note that the compositions shown in this section are converted to  $\mathbf{x}^b$  without the use of the MH-based method. Thus, the generated compositions include non-valid molecules (e.g.,  $\text{Li}_0.27\text{O}_0.72\text{Cr}_0.01$  in Table 1).

As shown in table 1,  $\text{CondGAN}(\mathbf{x}^{bp})$  generates certain compositions but not others. These generations may have been due to posterior collapse [29] and mode collapse [10]. These collapses are phenomena such that  $D_{KL}(q_\phi(\mathbf{z} | \mathbf{x}) || p(\mathbf{z})) = 0$  and the outputs of GANs degenerates to the mode. However, it is not yet clear why concatenating  $\mathbf{x}^p$  mitigates only CondGAN. A deeper analysis will constitute a future study.

Table 2 shows the mean absolute error (MAE), root mean squared error (RMSE), and distance  $d(\tilde{\mathbf{x}}, \text{near}(\tilde{\mathbf{x}})) / \dim(\tilde{\mathbf{x}})$ , where  $\tilde{\mathbf{x}}$  is the generated vector,  $\text{near}(\tilde{\mathbf{x}})$  is the nearest vector,  $d(\cdot, \cdot)$  is the Euclidean distance, and  $\dim(\tilde{\mathbf{x}})$  is the dimension of  $\tilde{\mathbf{x}}$ . MAE and RMSE are computed between the input property  $y$  and the nearest property  $\text{near}(y)$  corresponding to the property of  $\text{near}(\tilde{\mathbf{x}})$ . For references, we also evaluate the performances of  $\text{CondVAE}(\mathbf{x}^{bp})$  and  $\text{CondGAN}(\mathbf{x}^{bp})$  using only  $\mathbf{x}^b$ . As shown in table 2,  $\tilde{\mathbf{x}}$  that is generated by  $\text{CondGAN}(\mathbf{x}^{bp})$  is the closest to the real vector  $\text{near}(\tilde{\mathbf{x}})$  with the desired property.

Figure 1 (A) and table 3 show the histogram of  $\text{near}(y)$  by  $\text{CondGAN}(\mathbf{x}^{bp})$ , as well as examples of the generated and nearest compositions with input, predicted, and nearest properties. These results indicate that  $\text{CondGAN}(\mathbf{x}^{bp})$  generates compositions around the desired property despite the non-usage of crystal structures.

Table 1: Examples of generated inorganic compositions.

CondVAE( $\mathbf{x}^b$ )	CondVAE( $\mathbf{x}^{bp}$ )
Li0.09O0.65F0.08S0.09Se0.09	H0.09Li0.06O0.68F0.09S0.08
Li0.09O0.65F0.08S0.09Se0.09	H0.09Li0.06O0.68F0.09S0.08
Li0.09O0.65F0.08S0.09Se0.09	H0.09Li0.06O0.68F0.09S0.08
Li0.09O0.65F0.08S0.09Se0.09	H0.09Li0.06O0.68F0.09S0.08
Li0.09O0.65F0.08S0.09Se0.09	H0.09Li0.06O0.68F0.09S0.08
Li0.09O0.65F0.08S0.09Se0.09	H0.09Li0.06O0.68F0.09S0.08
Li0.09O0.65F0.08S0.09Se0.09	H0.09Li0.06O0.68F0.09S0.08
Li0.09O0.66F0.08S0.09Se0.08	H0.09Li0.06O0.68F0.09S0.08
Li0.09O0.66F0.08S0.08Se0.09	H0.09Li0.06O0.68F0.09S0.08
CondGAN( $\mathbf{x}^b$ )	CondGAN( $\mathbf{x}^{bp}$ )
F0.60As0.40	Li0.29O0.58Mn0.13
F0.92K0.04As0.04	Li0.27O0.72Cr0.01
O0.04F0.88K0.04Xe0.04	S0.01Pr0.59Sm0.40
O0.04F0.84K0.04As0.04Xe0.04	Li0.22O0.59Cr0.11Mn0.08
O0.05F0.83K0.04As0.04Xe0.04	S0.03Pr0.72Sm0.19U0.06
O0.06F0.81K0.05As0.04Xe0.04	O0.62Na0.09Ta0.01Au0.28
O0.06F0.81K0.05As0.04Xe0.04	S0.01Pr0.60Sm0.01Dy0.20U0.18
O0.06F0.81K0.05As0.04Xe0.04	H0.04C0.01O0.71Na0.24
O0.06F0.81K0.05As0.04Xe0.04	O0.85Ca0.11Ta0.01W0.02Au0.01

Table 2: Comparison of models. We compute MSE/RMSE between  $\text{near}(y)$  and  $y$ , as well as the distance  $d(\tilde{\mathbf{x}}, \text{near}(\tilde{\mathbf{x}}))/\dim(\tilde{\mathbf{x}})$ . We execute the random training/test data selection three times to compute (mean $\pm$ std).

		MAE	RMSE	Distance $\times 10^3$
CondVAE( $\mathbf{x}^b$ )		0.53 $\pm$ 0.11	0.64 $\pm$ 0.11	4.45 $\pm$ 0.07
CondGAN( $\mathbf{x}^b$ )		0.53 $\pm$ 0.05	0.68 $\pm$ 0.08	4.97 $\pm$ 0.43
CondVAE( $\mathbf{x}^{bp}$ )	$\mathbf{x}^b$	0.46 $\pm$ 0.13	0.60 $\pm$ 0.15	4.67 $\pm$ 0.36
	$\mathbf{x}^{bp}$	0.57 $\pm$ 0.11	0.74 $\pm$ 0.12	3.13 $\pm$ 0.06
CondGAN( $\mathbf{x}^{bp}$ )	$\mathbf{x}^b$	0.39 $\pm$ 0.01	0.52 $\pm$ 0.01	3.81 $\pm$ 0.11
	$\mathbf{x}^{bp}$	0.37 $\pm$ 0.03	0.46 $\pm$ 0.01	2.78 $\pm$ 0.07

## 6.2 Predicted Performance of Discriminator

As described in Sec.3.2, the discriminator of our CondGAN is able to predict not only real/fake but also property. Thus, we evaluate the performance of  $P(\cdot)$ .

Table 4 shows the MAE/RMSE of each CondGAN model. For comparison, we also show the performance of DNN, which has the same hyperparameters as the discriminator. CondGAN( $\mathbf{x}^{bp}$ ) provides better predictions than CondGAN( $\mathbf{x}^b$ ). Also, CondGAN( $\mathbf{x}^{bp}$ ) has a competitive performance to the standard DNN.

We speculate that  $P(\cdot)$  relates to the differences in the performances of the generative models. Thus, checking  $P(\cdot)$  may address the difficulty of checking the generative performances.

## 6.3 Valence Check and Modifications of Compositions

We evaluate the MH-based valency modification. Tables 5 and 6 show the evaluation performances of the MH-based modification and examples of the modified compositions. To compute these values, 10 properties ( $-4.49, -3.76, -3.45, -3.01, -2.50, -2.03, -1.52, -1.07, -0.48, \text{ and } -0.01$ ) are fed into CondGAN( $\mathbf{x}^{bp}$ ), which generates 256 samples per property.

As shown in Table 5, the MH-based modification reduces the violation of valency and the distance to the nearest composition while maintaining the performances of MAE/RMSE. However, we find compositions that cannot balance the atomic valency (e.g., Gd0.06Tb0.74Ac0.19 and Al0.10Ho0.90 in table 6) because the MH-based method is handled with only  $\mathbf{x}^b > TH$ . Intuitively speaking,

Table 3: Examples of generated compositions, predicted property  $P(\tilde{x})$ , nearest composition, and property of nearest composition  $\text{near}(y)$ . Note that the composition in parentheses of the nearest composition’s line is the normalized composition.

$y$	Generated composition	$P(\tilde{x})$	Nearest composition	$\text{near}(y)$
-3.25	O0.61Si0.01Ba0.38	-3.25	Ba9Sc2(SiO4)6 (O0.58Si0.15Sc0.05Ba0.22)	-3.46
-3.25	B0.04O0.65Ca0.30Sm0.01	-3.16	Ca5B3O9F (B0.17O0.50F0.06Ca0.28)	-3.40
-2.03	Li0.29O0.58Mn0.13	-2.02	Li4Mn5FeO12 (Li0.18O0.55Mn0.23Fe0.05)	-2.00
-2.03	Li0.27O0.72Cr0.01	-2.00	LiCr10O15 (Li0.04O0.58Cr0.38)	-2.23
-1.27	C0.02O0.98	-1.24	CrC5SO7 (C0.36O0.50S0.07Cr0.07)	-1.03
-1.27	Na0.80S0.04Cu0.16	-1.27	Na2S (Na0.67S0.33)	-1.26
-1.05	O0.34S0.05Zn0.61	-1.02	Zn3CdS4 (S0.50Zn0.38Cd0.12)	-1.08
-1.05	Ge0.02Cd0.10Eu0.02Er0.86	-1.13	ErGe (Ge0.50Er0.50)	-0.85
-0.10	Mg0.63Co0.01Sr0.10Dy0.26	-0.07	Dy5Mg24 (Mg0.83Dy0.17)	-0.04
-0.10	Zn0.10Cd0.89Hg0.01	-0.08	EuCd11 (Cd0.92Eu0.08)	-0.13

Table 4: Comparison of the performances of  $P(\cdot)$ . (mean $\pm$ std) is computed by the same random selection shown in table 2.

	CondGAN( $x^b$ )	CondGAN( $x^{bp}$ )	DNN
MAE	0.20 $\pm$ 0.00	0.12 $\pm$ 0.00	0.10 $\pm$ 0.01
RMSE	0.30 $\pm$ 0.01	0.20 $\pm$ 0.01	0.22 $\pm$ 0.03

applying the MH-based method to all dimensions can solve this problem, however such a solution is time-consuming. Thus, we will plan to constrain the atomic valency during the training phase of the generative model.

## 6.4 Extrapolation

Extrapolation is an important skill for finding compositions with desirable properties [22]. However, previous results cannot show the extrapolation performance because these evaluate only interpolated results. hence, we evaluate the extrapolation performance of CondGAN( $x^{bp}$ ) by changing the selection of training/test data.

Fig. 1 (B) shows the RMSE between  $y$  and  $\text{near}(y)$ . The generative performance becomes worse as the distance from the range of  $y$  increases. Also, the extrapolation performance becomes better when the range of  $y$  increases. This result implies that the functions of collecting and evaluating the outside data are indispensable. In the field of organic molecules, this function is implemented by RL techniques [31, 8]. However, as described in Sec. 1, achieving the reward efficiently is difficult for the generation of inorganic molecules. We intend to address this problem in a future study.

## 7 Conclusion and Future Works

In this study, we attempt to generate inorganic compositions without using crystal information. We construct four types of generative models and find that CondGAN( $x^{bp}$ ) perform the best. Also, we apply the MH-based modifications and show that this method is effective for balancing the atomic valency. Furthermore, we evaluate the extrapolation performance of CondGAN( $x^{bp}$ ) and confirm that the present generator can not generate chemical compositions while holding physical properties that lay outside the range of the properties included in the training data. The simplest way to overcome the difficulty is by collecting new data, including desired physical properties, in a broader range.

In the case of organic molecules, Alán Aspuru-Guzik et al. [12, 31] proposes an RL-based method to generate organic molecules by holding an optimized physical property even if that property lies outside of the initial training data. Such techniques for generators to optimize the physical properties of inorganic materials have not been achieved as far as we know and should be addressed in the future. Also, there should be improvements to the generative models and an analysis of why CondGAN( $x^{bp}$ ) works better.

Table 5: Evaluation of the MH-based valency modification. Raw represents the generated outputs of CondGAN( $x^{bp}$ ) and Modified represents the results of the MH-based modification.

	Valence	MAE	RMSE	Distance $\times 10^3$
Raw	$1.02 \pm 0.52$	$0.50 \pm 0.19$	$0.70 \pm 0.26$	$2.49 \pm 0.78$
Modified	$0.19 \pm 0.24$	$0.53 \pm 0.16$	$0.70 \pm 0.18$	$1.63 \pm 0.33$

Table 6: Examples of compositions modified by the MH-based algorithm.

Generated composition	Modified generated composition
O0.65Y0.11Ba0.04La0.20	O0.58Y0.12Ba0.12La0.18
O0.74La0.26	O0.60La0.40
O0.57La0.43	O0.60La0.40
O0.10F0.58Mg0.12Ba0.06Pr0.14	O0.10F0.58Mg0.12Ba0.06Pr0.14
Li0.07O0.53F0.09Co0.31	O0.50Co0.50
S0.84Ba0.16	S0.50Ba0.50
Li0.84O0.06Ni0.10	Li0.56O0.36Ni0.08
K0.06Se0.65In0.11Cs0.18	Se0.38In0.07Cs0.55
Ce0.25Gd0.15Tb0.11Ir0.16Ac0.27Th0.06	Gd0.06Tb0.74Ac0.19
Al0.85Ho0.15	Al0.10Ho0.90

## Acknowledgments

We would like to thank Mila members for their useful input and discussion.

## References

- [1] <https://github.com/yoshida-lab/XenonPy>.
- [2] <https://www.tensorflow.org/>.
- [3] Rim Assouel et al. "Defactor: Differentiable edge factorization-based probabilistic graph generation". In: *arXiv preprint arXiv:1811.09766* (2018).
- [4] Christopher M Bishop. *Pattern recognition and machine learning*. springer, 2006.
- [5] Xavier Bresson and Thomas Laurent. "A Two-Step Graph Convolutional Decoder for Molecule Generation". In: *arXiv preprint arXiv:1906.03412* (2019).
- [6] Andrew Brock, Jeff Donahue, and Karen Simonyan. "Large scale gan training for high fidelity natural image synthesis". In: *arXiv preprint arXiv:1809.11096* (2018).
- [7] Chi Chen et al. "Graph networks as a universal machine learning framework for molecules and crystals". In: *Chemistry of Materials* 31.9 (2019), pp. 3564–3572.
- [8] Nicola De Cao and Thomas Kipf. "MolGAN: An implicit generative model for small molecular graphs". In: *arXiv preprint arXiv:1805.11973* (2018).
- [9] Rafael Gómez-Bombarelli et al. "Automatic chemical design using a data-driven continuous representation of molecules". In: *ACS central science* 4.2 (2018), pp. 268–276.
- [10] Ian Goodfellow. "NIPS 2016 tutorial: Generative adversarial networks". In: *arXiv preprint arXiv:1701.00160* (2016).
- [11] Ian Goodfellow et al. "Generative adversarial nets". In: *Advances in neural information processing systems*. 2014, pp. 2672–2680.
- [12] Gabriel Lima Guimaraes et al. "Objective-reinforced generative adversarial networks (ORGAN) for sequence generation models". In: *arXiv preprint arXiv:1705.10843* (2017).
- [13] Ishaan Gulrajani et al. "Improved training of wasserstein gans". In: *Advances in Neural Information Processing Systems*. 2017, pp. 5767–5777.
- [14] Jordan Hoffmann et al. "Data-Driven Approach to Encoding and Decoding 3-D Crystal Structures". In: *arXiv preprint arXiv:1909.00949* (2019).
- [15] Anubhav Jain et al. "Commentary: The Materials Project: A materials genome approach to accelerating materials innovation". In: *Apl Materials* 1.1 (2013), p. 011002.

- [16] Avni Jain, Jonathan A Bollinger, and Thomas M Truskett. “Perspective: Inverse methods for material design”. In: *arXiv preprint arXiv:1405.4060* (2014).
- [17] Diederik P Kingma and Max Welling. “Auto-encoding variational bayes”. In: *arXiv preprint arXiv:1312.6114* (2013).
- [18] Durk P Kingma et al. “Semi-supervised learning with deep generative models”. In: *Advances in neural information processing systems*. 2014, pp. 3581–3589.
- [19] Jack Kllys, Jake Snell, and Richard Zemel. “Learning latent subspaces in variational autoencoders”. In: *Advances in Neural Information Processing Systems*. 2018, pp. 6444–6454.
- [20] Jaechang Lim et al. “Molecular generative model based on conditional variational autoencoder for de novo molecular design”. In: *Journal of cheminformatics* 10.1 (2018), p. 31.
- [21] Kaushalya Madhawa et al. “GraphNVP: An Invertible Flow Model for Generating Molecular Graphs”. In: *arXiv preprint arXiv:1905.11600* (2019).
- [22] Bryce Meredig et al. “Can machine learning identify the next high-temperature superconductor? Examining extrapolation performance for materials discovery”. In: *Molecular Systems Design & Engineering* 3.5 (2018), pp. 819–825.
- [23] Mehdi Mirza and Simon Osindero. “Conditional generative adversarial nets”. In: *arXiv preprint arXiv:1411.1784* (2014).
- [24] Juhwan Noh et al. “Inverse Design of Solid-State Materials via a Continuous Representation”. In: *Matter* (2019). ISSN: 2590-2385.
- [25] Asma Nouira, Jean-Claude Crivello, and Nataliya Sokolovska. “CrystalGAN: Learning to Discover Crystallographic Structures with Generative Adversarial Networks”. In: *arXiv preprint arXiv:1810.11203* (2018).
- [26] Augustus Odena, Christopher Olah, and Jonathon Shlens. “Conditional Image Synthesis with Auxiliary Classifier GANs”. In: *International Conference on Machine Learning*. 2017, pp. 2642–2651.
- [27] Shyue Ping Ong et al. “Python Materials Genomics (pymatgen): A robust, open-source python library for materials analysis”. In: *Computational Materials Science* 68 (2013), pp. 314–319.
- [28] Aaron van den Oord et al. “Wavenet: A generative model for raw audio”. In: *arXiv preprint arXiv:1609.03499* (2016).
- [29] Ali Razavi et al. “Preventing posterior collapse with delta-vaes”. In: *arXiv preprint arXiv:1901.03416* (2019).
- [30] Benjamin Sanchez-Lengeling and Alán Aspuru-Guzik. “Inverse molecular design using machine learning: Generative models for matter engineering”. In: *Science* 361.6400 (2018), pp. 360–365.
- [31] Benjamin Sanchez-Lengeling et al. “Optimizing distributions over molecular space. An objective-reinforced generative adversarial network for inverse-design chemistry (ORGANIC)”. In: (2017).
- [32] Kristof T Schütt et al. “SchNet—A deep learning architecture for molecules and materials”. In: *The Journal of Chemical Physics* 148.24 (2018), p. 241722.
- [33] Daniel Schwalbe-Koda and Rafael Gómez-Bombarelli. “Generative Models for Automatic Chemical Design”. In: *arXiv preprint arXiv:1907.01632* (2019).
- [34] Atsuto Seko et al. “Representation of compounds for machine-learning prediction of physical properties”. In: *Physical Review B* 95.14 (2017), p. 144110.
- [35] Tian Xie and Jeffrey C Grossman. “Crystal graph convolutional neural networks for an accurate and interpretable prediction of material properties”. In: *Physical review letters* 120.14 (2018), p. 145301.



## Appendix

Table A: List of physical descriptors. These 58 descriptors of 94 atoms (from H to Pu) have been saved in the Xenonpy library [1].

Descriptors
Period in the periodic table
Number of protons found in the nucleus of an atom
Atom number in mendeleev's periodic table
Atomic radius
Atomic radius by Rahm et al
Atomic volume
The mass of an atom
Atom volume in ICSD database
physical dimension of unit cells in a crystal lattice
Van der Waals radius
Van der Waals radius according to Alvarez
Van der Waals radius according to Batsanov
Van der Waals radius according to Bondi
Van der Waals radius from the DREIDING FF
Van der Waals radius from the MM3 FF
Van der Waals radius according to Rowland and Taylor
Van der Waals radius according to Truhlar
Van der Waals radius from the UFF
Covalent radius by Bragg
Covalent radius by Cerdero et al
Single bond covalent radius by Pyykko et al
Double bond covalent radius by Pyykko et al
Triple bond covalent radius by Pyykko et al
Covalent radius by Slater
$C_6$ dispersion coefficient in a.u
$C_6$ dispersion coefficient in a.u
Density at 295K
Proton affinity
Dipole polarizability
Electron affinity
Tendency of an atom to attract a shared pair of electrons
Allen's scale of electronegativity
Ghosh's scale of electronegativity
Mulliken's scale of electronegativity
DFT bandgap energy of T=0K ground state
Estimated FCC lattice parameter based on the DFT volume
Estimated BCC lattice parameter based on the DFT volume
Estimated FCC lattice parameter based on the DFT volume
DFT magnetic moment of T=0K ground state
DFT volume per atom of T=0K ground state
Herfindahl-Hirschman Index (HHI) production values
Herfindahl-Hirschman Index (HHI) reserves values
Specific heat at 20oC
Gas basicity
First ionisation energy
Fusion heat
Heat of formation
Mass specific heat capacity
Molar specific heat capacity
Evaporation heat

Coefficient of linear expansion
Boiling temperature
Brinell Hardness Number
Bulk modulus
Melting point
Single-bond metallic radius
Metallic radius with 12 nearest neighbors
Thermal conductivity at 25 C
Speed of sound
Value of Vickers hardness test
Ability to form instantaneous dipoles
Young's modulus
Poisson's ratio
Molar volume
Total unfilled electron
Total valance electron
Unfilled electron in d shell
Valance electron in d shell
Unfilled electron in f shell
Valance electron in f shell
Unfilled electron in p shell
Valance electron in p shell
Unfilled electron in s shell
Valance electron in s shell

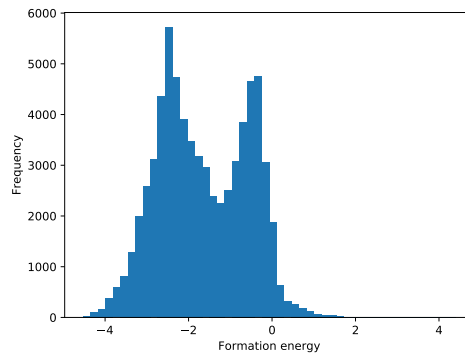


Figure A: Histogram of the formation energies [eV/atom] in the Materials Project.